Comprehensive Model for Allosteric Regulation of Mammalian Ribonucleotide Reductase: Refinements and Consequences†

Ossama B. Kashlan‡ and Barry S. Cooperman*

Department of Chemistry, University of Pennsylvania, Philadelphia, Pennsylvania 19104-6323

Received October 25, 2002; Revised Manuscript Received December 12, 2002

ABSTRACT: Reduction of NDPs by murine ribonucleotide reductase (mRR) requires catalytic (mR1) and free radical-containing (mR2) subunits and is regulated by nucleoside triphosphate allosteric effectors. Here we present the results of several studies that refine the recently presented comprehensive model for the allosteric control of mRR enzymatic activity [Kashlan, O. B., et al. (2002) *Biochemistry 41*, 462−474], in which nucleotide binding to the specificity site (s-site) drives formation of an active $R1_2R2_2$ dimer, ATP or dATP binding to the adenine site (a-site) drives formation of a tetramer, $mR1_{4a}$, which isomerizes to an inactive form, $mR1_{4b}$, and ATP binding to the hexamerization site (h-site) drives formation of an active $R1_6R2_6$ hexamer. Analysis of the a-site D57N variant of mR1, which differs from wild-type mR1 (wt-mR1) in that its RR activity is activated by both ATP and dATP, demonstrates that dATP activation of the D57N variant RR arises from a blockage in the formation of $mR1_{4b}$ from $mR1_{4a}$, and provides strong evidence that $mR1_{4a}$ forms active complexes with $mR2_2$. We further demonstrate that (a) differences in the effects of ATP versus dATP binding to the a-site of wt-mR1 provide specific mechanisms by which the dATP/ATP ratio in mammalian cells could modulate in vivo RR enzymatic activity, (b) the comprehensive model is valid over a range of Mg^{2+} concentrations that include in vivo concentrations, and (c) equilibrium constants derived for the comprehensive model can be used to simulate the distribution of R1 among dimer, tetramer, and hexamer forms in vivo. Such simulations indicate that $mR1_6$ predominates over $mR1_2$ in the cytoplasm of normal mammalian cells, where the great majority of RR activity is located, but that $mR1_2$ may be important for nuclear RR activity and for RR activity in cells in which the level of ATP is depleted.

Ribonucleotide reductases (RRs)[1] are allosterically regulated enzymes that catalyze the conversion of ribonucleotides to 2′-deoxyribonucleotides (*1*), providing the deoxynucleotide substrates that are essential for de novo DNA biosynthesis. Class Ia RRs, which comprise all eukaryotic RRs as well as some from eubacteria, bacteriophages, and viruses (*1*), accept the four common nucleoside diphosphates (NDPs) as substrates, with enzymatic activity being dependent upon the formation of a complex between two different subunits, R1 and R2. The R2 subunit contains a stable tyrosyl free radical that is necessary for NDP reduction (*2*). The enzymatic active site, and all sites for allosteric ligands, are located on the R1 subunit.

Recently (*3*, *4*), we presented a comprehensive model for allosteric regulation of mammalian ribonucleotide reductase (mRR), based on molecular mass, ligand binding, and activity studies, that accounts quantitatively for the modulation of RR enzymatic activity toward all four NDP substrates by the four allosteric ligands ATP, dATP, dGTP, and dTTP. The major features of this model, which makes clear the centrality of ligand-dependent changes in R1 quaternary structure for mRR regulation and is presented in simplified form in Scheme 1, may be summarized as follows.

(1) The R1 subunit contains three different allosteric sites, the s-, a-, and h-sites. At physiologically important concentrations, all four allosteric ligands bind to the s-site, only dATP and ATP bind to the a-site, and only ATP binds to the h-site.

(2) Unliganded mR1 is preferentially a monomer. Binding of any of the four allosteric ligands to the s-site (dissociation constant, K_L) drives $mR1_2$ formation.

(3) Binding to the s-site also dictates substrate selection. Thus, binding of either ATP or dATP stimulates the reduction of both CDP and UDP; binding of dTTP stimulates the reduction of GDP, and binding of dGTP stimulates the reduction of ADP. Such specificity in substrate reduction results primarily from the effects on k_{cat} (an allosteric V-system) rather than from effects on K_m (an allosteric K-system). The same or very similar specific pairwise interactions are preserved in class Ib, II, and III RRs, with a recent X-ray structure of a class III RR providing explicit evidence for how conformational changes induced by allosteric ligand binding to the s-site are propagated directly to the active site (*5*). At physiological concentrations, the s-site is saturated, with occupancy governed by competition among ATP, dATP, dTTP, and dGTP.

† Supported by NIH Grant CA58567.

* To whom correspondence should be addressed. Telephone: (215) 898-6330. Fax: (215) 898-2037. E-mail: cooprman@pobox.upenn.edu.

‡ Current address: Department of Medicine, University of Pittsburgh, Pittsburgh, PA 15261.

[1] Abbreviations: DLS, dynamic light scattering; mR1, large subunit of murine ribonucleotide reductase; mR2, small subunit of murine ribonucleotide reductase; mRR, murine ribonucleotide reductase; NDPs, nucleoside diphosphates; RR, ribonucleotide reductase.

10.1021/bi020634d CCC: $25.00
Published on Web 01/24/2003

Scheme 1: Allosteric Ligand Effects on Enzyme Aggregation State and Activity[a]

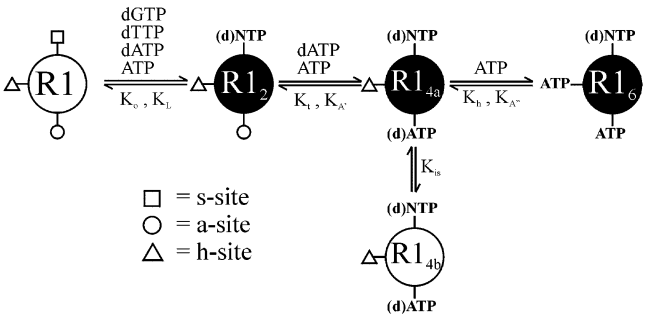

[a] R2 has been omitted for simplicity; activity assays were carried out in the presence of saturating R2 concentrations. States shown filled in black have high activity, while those filled in white have little or no activity. For wt-mR1, equilibration is slow when ATP occupies the a-site. For D57N-mR1, $R1_{4b}$ formation is blocked.

(4) Binding of either ATP or dATP to the a-site (dissociation constant, $K_{A'}$) drives formation of $mR1_4$. $mR1_4$ exists in two conformations, $mR1_{4a}$ and $mR1_{4b}$, with the latter predominating at equilibrium. At physiological concentrations, the a-site is saturated, with occupancy governed by competition between ATP and dATP.

(5) ATP binding to the h-site (dissociation constant, $K_{A''}$) drives formation of $mR1_6$.

(6) The $R2_2$ complexes of both $mR1_2$ (i.e., $mR1_2R2_2$) and $mR1_6$ (i.e., $mR1_6R2_6$) are enzymatically active, whereas the $R2_2$ complex $mR1_{4b}$ has little if any activity. Left unspecified in our earlier model is the activity of the $R2_2$ complex of $mR1_{4a}$.

(7) $R2_2$ has nearly identical affinity for binding either to one site on $R1_2$ or to three equivalent sites on $R1_6$ and, with the exception of K_o, has no major effects on the equilibrium constants (Table 1) that characterize Scheme 1 (*4*).

(8) The well-known phenomenon that dATP inhibits all NDP reductase activity derives from its induction of $mR1_{4b}$ formation. In contrast, measured at high concentrations, ATP is a general activator of NDP reductase activity because it induces $mR1_6$ formation.

(9) The concentrations of ATP found in mammalian cells are quite similar to those required, under a variety of conditions, for converting $mR1_{4b}$ to $mR1_6$, leading to the suggestion that $mR1_6R2_j$ ($j = 2$, 4, or 6) is the major active form of RR in such cells.

The comprehensive model represents an important revision of the earlier phenomenological model of Reichard and Thelander (*1*, *6*, *7*), which ignored effects of $R1_4$ and $R1_6$ formation on RR activity and did not include the h-site.

Here we report the results of several studies carried out to further refine and explore the consequences of the comprehensive model. A major focus of our work is the variant D57N-mR1, originally isolated from a mouse T-lymphoma cell line that is resistant to growth inhibition by deoxyadenosine (*8*, *9*), which differs from wild-type mR1 (wt-mR1) in that its RR activity is activated by both ATP and dATP (*7*). Asp57 in mR1 aligns with His59 in *Escherichia coli* R1 (eR1), an amino acid residue that has been shown by X-ray crystallography to be part of the a-site and to fall within the R1 dimer−dimer contact region (*4*, *10*, *11*) (PDB entry 1RLR). The analysis of D57N-mR1 focuses on the effects of ATP and dATP on mR1 aggregation and RR activity in the presence of the substrates GDP and CDP, it having previously been shown for wt-mR1 that such effects are very similar for the purine substrates GDP and ADP and for the pyrimidine substrates CDP and UDP (*4*). Our results indicate that dATP activation of the D57N variant RR arises from a blockage in the formation of $mR1_{4b}$ from $mR1_{4a}$, and that $mR1_{4a}$ forms active complexes with $R2_2$.

Other results, reported below, demonstrate a clear difference in the consequences of a-site binding of ATP versus dATP on the functional properties of $mR1_6$, use the equilibrium constants derived for Scheme 1 to simulate the distribution of R1 among dimer, tetramer, and hexamer forms in vivo, and make clear the rather weak dependence of mR1 oligomerization and mRR activity on Mg^{2+} concentration.

EXPERIMENTAL PROCEDURES

Materials

Recombinant wt-mR1 and mR2 were prepared as described previously (*3*). All other materials were of the highest available purity.

Expression and Purification of D57N-mR1. The D57N-mR1 protein was expressed in Bl21(DE3)pLysS bacteria containing the pETD57NR1 vector (gift of L. Thelander) as previously described (*7*, *12*, *13*). D57N-mR1 was purified using a procedure previously described for wt-mR1 (*3*) with the following modifications. Cells were suspended in 50 mM Tris-HCl (pH 7.6) and 0.1 mM dithiothreitol (DTT) (buffer A) with added protease inhibitors (1 μM leupeptein and aprotinin) and lysed by two passages through a French pressure cell (10000−12000 psi). After the Sephadex-G25 step, protein fractions devoid of ammonium sulfate were pooled and loaded directly onto a preequilibrated FTLDADF-Sepharose affinity column (*14*) (1.3 $cm^2 \times 11$ cm, 0.5 mL/min). Nonspecifically bound protein was eluted from the column with buffer A and monitored by A_{280}. Specifically bound protein was eluted with buffer A containing 0.5 M KCl, conditions under which two protein peaks were observed. Peak 1 eluted immediately upon addition of buffer A containing 0.5 M KCl and contained D57N-mR1 and impurities (Figure 1, lane 5). Peak 2 eluted 22 min after the addition of buffer A with 0.5 M KCl, continued for approximately 120 min, and contained pure D57N-mR1 (Figure 1, lane 6). The large height/diameter ratio of the column was required for resolution of peak 2 from peak 1. Peak 2 was dialyzed overnight at 4 °C against buffer A with 0.1 M KCl, concentrated to approximately 4 mg/mL, quick frozen in liquid N_2, and stored at −80 °C. Peak 1, which forms aggregates that interfere with dynamic light scattering measurements, was discarded. The overall yield of peak 2 protein was 0.2 mg/g of cells. Purified D57N-mR1 was stable for at least several months at −80 °C and several hours at 25 °C.

Methods

Determinations of protein and nucleotide concentrations and of nucleotide purity and assays of enzyme activity were carried out at 25 °C, as previously described (*3*). For the assays, all components of the reaction mixture were preincubated for 7 min prior to substrate addition except as otherwise indicated. All enzyme activity data are reported

Table 1: Equations for Equilibrium Constants and Measurements

equilibrium constant

$$K_L = 2[R1_2][L]/[R1_2L] = 0.5[R1_2L][L]/[R1_2L_2] \quad (1)$$ for s-site binding

$$K_{A'} = 4[R1_{4a}L_i][A]/[R1_{4a}L_iA'] = 0.25[R1_{4a}L_iA'_3][A]/[R1_{4a}L_iA'_4] \text{ where } i = 0-4 \quad (2)$$ for a-site binding

$$K_{A''} = 6[R1_6L_iA'_j][A]/[R1_6L_iA'_jA''] = {}^1/_6[R1_6L_iA'_jA''_5][A]/[R1_6L_iA'_jA''_6] \text{ where } i \text{ and } j = 0-6 \quad (3)$$ for h-site binding

$$K_o = [R1]^2/[R1_2] \quad (4)$$

$$K_t = [R1_2]^2/[R1_{4a}] = [R1_2L_2]^2/[R1_{4a}L_4] \quad (5)$$

$$K_h = [R1_2][R1_{4a}]/[R1_6] \quad (6)$$

$$K_{is} = [R1_{4b}]/[R1_{4a}] \quad (7)$$

definitions

$\alpha = [L]/K_L$; $\beta = [A]/K_{A'}$; $\gamma = [A]/K_{A''}$; α_{dNTP} is defined equivalently for a specific dNTP

DLS measurements

$$M_{obsd} = \frac{90\ \text{kDa}}{[R1]_T}([R1]_t + 4[R1_2]_t + 16[R1_4]_t + 36[R1_6]_t) \quad (8)$$

activity measurements

k_{cat} values for $R2_2$ complexes of $R1_2$, $R1_{4a}$, $R1_{4b}$, and $R1_6$ are k_d, k_{4a}, k_{4b}, and k_h, respectively

GDP or CDP reductase

$$v = \frac{1}{[R1]_T}\left[2k_d[R1_2]_t + 4\frac{k_d(1+K_{is}) + (k_{4a}+k_{4b}K_{is})\beta(2+\beta)}{(1+K_{is})(1+\beta)^2}[R1_4]_t + 6\frac{(k_{4b}+k_h\gamma)(2+\gamma)}{(1+\gamma)^2}[R1_6]_t\right] \quad (9)$$

GDP reductase with competing dATP if the hybrid [one bound dATP and one bound dGTP (see text)] is inactive

$$v' = \frac{\alpha_{dTTP}(2+\alpha_{dTTP})}{(1+\alpha_{dATP}+\alpha_{dTTP})^2}v \quad (10)$$

if the hybrid is active

$$v' = \frac{\alpha_{dTTP}(2+2\alpha_{dATP}+\alpha_{dTTP})}{(1+\alpha_{dATP}+\alpha_{dTTP})^2}v \quad (11)$$

simulations

$$[R1]_T = [R1]_t + 2[R1_2]_t + 4[R1_4]_t + 6[R1_6]_t \quad (12)$$

where $[R1]_t$, $[R1_2]_t$, $4[R1_4]_t$, and $[R1_6]_t$ are concentrations of all forms of monomer, dimer, tetramer, and hexamer, respectively, in solution (*4*)

$$f(R1_n) = n[R1_n]/([R1]_T - [R1]) \text{ where } n = 2, 4, \text{ or } 6 \quad (13)$$

as the average of duplicate measurements ± the average deviation. wt-mR1, D57N-mR1, and mR2 concentrations are reported as monomer concentrations.

Dynamic Light Scattering (DLS). Samples (60 μL) were prepared in 50 mM hydroxyethylpiperazineethanesulfonic acid (HEPES) (pH 7.6), 25 mM DTT, 10 mM KCl, and 10 mM $MgCl_2$, unless otherwise indicated, with R1 and ligand (effector and/or substrate) concentrations as indicated. Samples were then centrifuged at 15000*g* for 10 min and then filtered through 0.1 μm Ultrafree-MC (Millipore) filters at 9000*g* for 3 min to remove dust and particulate matter. DLS measurements were made with a DynaPro 99 P dynamic light scattering instrument (Protein Solutions) at 25.0 °C.

Equations for Curve Fitting and Simulation. Except as otherwise indicated, all DLS and activity data in Figures 2−4 were fit to eqs 8 and 9 (Table 1), respectively, using Igor Pro 3.16 (Wavemetrics, Oswego, OR) and a curve fitting procedure as previously described (*4*). Activity data for D57N-mR1 in Figure 3B were fit to both eqs 10 and 11 (Table 1).

Simulations of the distribution of mR1 among dimer, tetramer, and hexamer forms complexed with $mR2_2$, as a function of $[R1]_T$, [ATP], and [dATP], were carried out using eqs 12 and 13. The values (*4*) used for intrinsic R1 oligomer dissociation constants K_o, K_t, and K_h were 5, 5900, and 1.7 μM, respectively, and the value used for R1 tetramer isomerization, K_{is}, was 40. The values for ATP dissociation constants K_L, $K_{A'}$, and $K_{A''}$ were 100, 100, and 2000 μM, respectively. The values for dATP dissociation constants K_L and $K_{A'}$ were both 1 μM.

RESULTS

Below we report results for DLS measurements of the apparent R1 molecular mass, carried out in the absence of mR2, and of the ribonucleotide reductase enzymatic activity, carried out in the presence of saturating mR2, except as otherwise indicated.

Effect of the D57N Mutation on dTTP Modulation of GDP Reductase and mR1 Dimerization. As with wt-mR1 (*3*), dTTP induces both dimerization of D57N-mR1 and GDP reductase activity (Figure 2). Although the affinity of dTTP

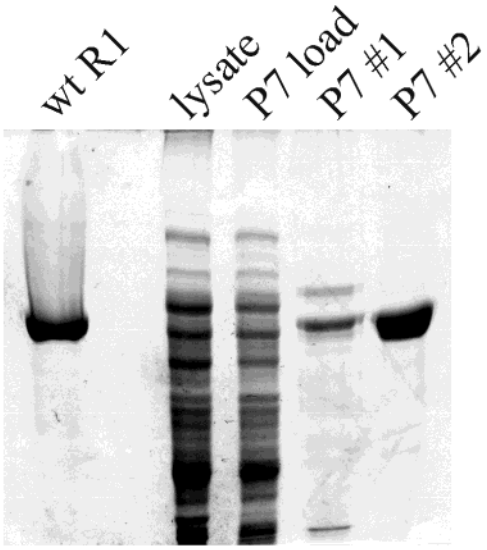

FIGURE 1: Purification of D57N-mR1. SDS−PAGE with a 7.5% acrylamide gel: lane 1, wt-mR1; lane 2, empty; lane 3, cell lysate; lane 4, sample loaded onto a FTLDADF−Sepharose (P7) column; lane 5, peak 1 from 0.5 M KCl elution; and lane 6, peak 2 from 0.5 M KCl elution.

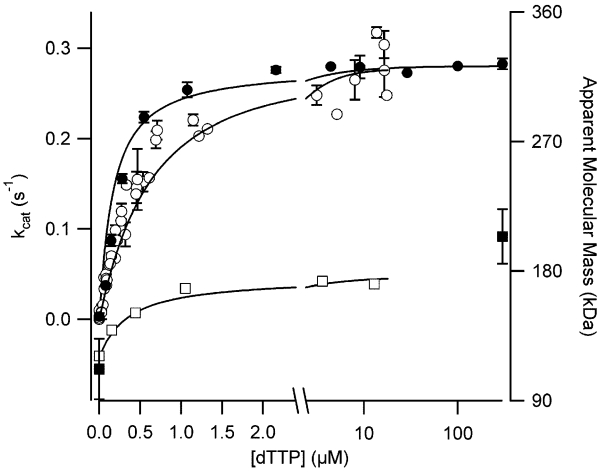

FIGURE 2: Dependence of GDP reductase and R1 molecular mass on dTTP concentration. All solutions contained varying dTTP concentrations as shown. Solutions for measuring GDP reductase activity contained 1.0 μM wt-mR1, 2.3 μM R2, and 1 mM GDP (○) or 1.2 μM D57N-mR1, 2.0 μM R2, and 600 μM GDP (●). Solutions for measuring the molecular mass of R1 contained 7.0 μM wt-mR1 and 1 mM GDP (□) or 5.0 μM D57N-mR1 and 600 μM GDP (■).

for the s-site is increased approximately 10-fold as a result of the D57N mutation (Table 2), the specific activities of dTTP-dependent wt- and D57N-GDP reductases are essentially identical (Table 3).

Effect of the D57N Mutation on ATP or dATP Modulation of GDP Reductase and mR1 Aggregation. ATP modulates both the GDP reductase activity (Figure 3A) and the state of aggregation (Figure 3C) of both wt- and D57N-mR1 containing s-site-bound dTTP. At low concentrations, ATP inhibits dTTP-dependent wt-GDP reductase, concomitant with inducing wt-mR1 tetramer formation, reaching a minimum at approximately 0.5 mM ATP. At higher concentrations, ATP almost completely restores reductase activity, concomitant with inducing wt-mR1 hexamer formation. The D57N mutation, while having only minor effects on ATP-induced mR1 aggregation, dramatically alters the ATP

Table 2: Dissociation Constants (μM)

constant	ligand	wild type[a] (dTTP)/GDP	D57N (dTTP)/GDP	wild-type[a] CDP	D57N CDP
K_t		5900 ± 100	45 ± 5	5900 ± 100	45 ± 5
K_h		1.7 ± 0.1	125 ± 7	1.7 ± 0.1	125 ± 7
K_L (s)	dTTP	1.4[b]	0.1 ± 0.01		
K_L (s)	ATP			25 ± 1	4.7 ± 1.3
$K_{A'}$ (a)		140 ± 10	21 ± 2	300 ± 10	96 ± 14
$K_{A''}$ (h)		4200 ± 100	1510 ± 16	2200 ± 100	4000 ± 100
K_L (s)	dATP		0.50 ± 0.01[d] 0.079 ± 0.001[e]	0.66 ± 0.02	0.9 ± 0.4
$K_{A'}$ (a)		0.96 ± 0.01 (1.7 ± 0.1)[c]	8.0 ± 0.2	0.30 ± 0.01	90 ± 15
$K_{A''}$ (h)				61000 ± 7000	

[a] From Kashlan et al. (*4*) unless otherwise indicated. [b] From Scott et al. (*3*). [c] No added GDP. [d] Competition with dTTP, hybrid inactive, eq 10. [e] Competition with dTTP, hybrid active, eq 11.

effects on dTTP-dependent GDP reductase specific activity, which now increases from 0.28 to 0.40 s^{-1} as the ATP concentration is increased to 500 μM and then decreases as the ATP concentration is further increased, reaching a plateau value of 0.30 s^{-1} at 3 mM ATP.

dTTP-dependent GDP reductase (Figure 3B) and mR1 aggregation (Figure 3D) are also modulated by dATP. For wt-mR1, dATP inhibits reductase activity, concomitant with mR1 tetramer formation, in processes that are virtually complete at a dATP concentration of 5 μM. For D57N-mR1, in contrast, dATP-induced R1 tetramer formation is accompanied by an increase in GDP reductase activity, with k_{cat} increasing from 0.28 to 0.42 s^{-1}. Moreover, these changes require a dATP concentration (~50 μM) considerably higher than that for wt-mR1. GDP reductase activity then falls as the dATP concentration is further increased, reaching a value of 0.09 s^{-1} at 3 mM dATP. This activity reduction does not coincide with a change in the apparent molecular mass of D57N-mR1, and can be attributed to dATP displacement of dTTP from the s-site.

These latter results were fit to different cooperative models for s-site binding, which assume that a hybrid R1 dimeric unit in which one s-site contains dTTP while the other is filled with dATP has either 0% (eq 10) or 100% (eq 11) GDP reductase activity. A third possibility, that the hybrid dimer has half-activity toward GDP reduction, was rejected on the basis of earlier results which provided strong evidence against such a noncooperative model (*3*). Adequate fits were obtained to either eq 10 or 11, yielding K_L values for dATP binding to the s-site of 0.50 or 0.08 μM, respectively. Comparing these K_L values with the value of 0.9 ± 0.4 μM (Table 2) obtained in the presence of CDP (see below) and the absence of both dTTP and GDP leads to the conclusion that the hybrid dimer is likely to be completely inactive as a GDP reductase (eq 10), since a noncognate substrate (GDP) bound to the active site should, if anything, decrease the affinity of dATP for the s-site as compared with the effect of a cognate substrate (CDP) (*3*, *15*, *16*).

Effect of the D57N Mutation on ATP or dATP Modulation of CDP Reductase and mR1 Aggregation. Added in the presence of CDP, ATP modulates CDP reductase activity (Figure 4A) and mR1 aggregation (Figure 4C). The CDP reductase activity of wt-mR1 shows clear triphasic dependence as a function of ATP concentration, with an increase in activity associated with mR1 dimer formation, a large decrease associated with mR1 tetramer formation, and an

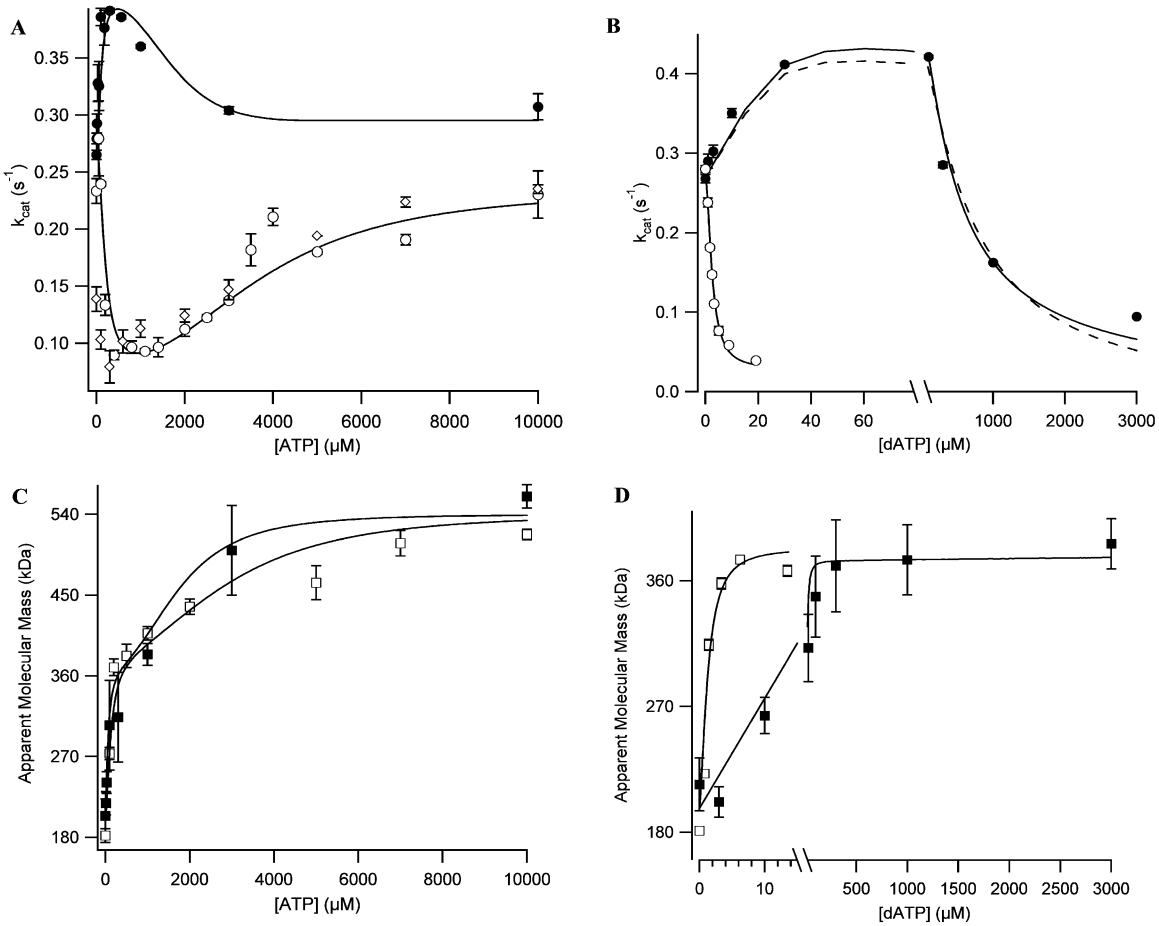

FIGURE 3: Dependence of dTTP-dependent GDP reductase and R1 molecular mass on ATP or dATP concentration. All solutions contained 10 mM Mg^{2+}, except as otherwise indicated, and varying ATP or dATP concentrations as shown. Solutions for measuring GDP reductase activity also contained 1.2 μM D57N-mR1 or 1.2 μM wt-mR1 and 2.0 μM R2, except as otherwise indicated. (A) GDP reductase vs ATP. All solutions contained 300 μM dTTP: wt-mR1 and 100 μM GDP (○), wt-mR1, 3 mM Mg^{2+}, and 600 μM GDP (◇), and D57N-mR1 and 600 μM GDP (●). (B) GDP reductase vs dATP: 2.0 μM wt-mR1, 20 μM R2, 100 μM dTTP, and 1 mM GDP (○) and D57N-mR1, 300 μM dTTP, and 600 μM GDP (●). (C) R1 molecular mass vs ATP. All solutions contained 300 μM dTTP: 5.7 μM wt-mR1 and 100 μM GDP (□) and 5.0 μM D57N-mR1 and 600 μM GDP (■). (D) R1 molecular mass vs dATP: 980 μM dTTP, no GDP, and 6.1 μM wt-mR1 (□) and 300 μM dTTP, 600 μM GDP, and 5.0 μM D57N-mR1 (■). Each point is the average of two measurements ± the average deviation. D57N-mR1 data sets for panels A and C were fit simultaneously using Scheme 1, as were D57N-mR1 data sets for panels B and D. In panel B, the dashed line is a fit to eq 10 and the solid line is a fit to eq 11. Data for wt-mR1 at 10 mM Mg^{2+} and the corresponding solid line fits have been reprised from Kashlan et al. (*4*).

increase back up to the dimer level associated with mR1 hexamer formation. For D57N-mR1, tetramer formation occurs at a considerably lower ATP concentration, resulting in a much clearer demonstration of the tetramer intermediate state. In addition, in contrast with that of wt-mR1, the CDP reductase specific activity shows little dependence on the aggregation state of D57N-mR1.

dATP also modulates CDP reductase activity (Figure 4B) and mR1 aggregation in the presence of CDP (Figure 4D). wt-mR1 reductase activity initially increases with added dATP, corresponding to mR1 dimer formation, and then decreases almost to zero (<5%) as the dATP concentration is increased further and the mR1 tetramer is formed. D57N-mR1 CDP reductase activity also increases with dATP-induced dimer formation but, in contrast to that of wt-mR1, undergoes a much more modest loss of activity on D57N-mR1 tetramer formation. A further difference is that much higher levels of dATP are required for tetramer formation.

Effect of the D57N Mutation on the Loss of GDP Reductase Activity during Preincubation. Shown in Figure 5 are the effects of varying the time of preincubation (0−30 min) on dTTP-dependent GDP reductase for both wt-mR1 ($[Mg^{2+}]_T$, 3 or 10 mM) and D57N-mR1 ($[Mg^{2+}]_T$, 10 mM). These experiments were carried out either in the absence of ATP (Figure 5A), where the mR1 dimer prevails, at 0.5 mM ATP (Figure 5B), giving maximum mR1 tetramer formation, or at 10 mM ATP (Figure 5C), affording the mR1 hexamer. Earlier (*4*), we showed that, at 10 mM Mg^{2+}, wt-mR1 activity decreased rather rapidly and reversibly in the presence of 0.5 mM ATP, which contrasted with much slower decreases (denoted ATP-independent) seen at either 0 or 10 mM ATP. The rapid decrease was attributed to the isomerization of an initially formed tetramer, $R1_{4a}$, which we now have shown to be enzymatically active (Table 3), to an enzymatically inactive tetramer, $R1_{4b}$ (Scheme 1). The results presented here demonstrate that the D57N mutation abolishes the rapid loss of reductase activity by the mR1 tetramer, suggesting that the mutation prevents $R1_{4b}$ formation. They also show that reducing $[Mg^{2+}]_t$ from 10 to 3 mM significantly decreases both the rate constant for rapid activity loss (from 0.24 to 0.11 min^{-1}, Figure 5B) and the rate constants for the slower ATP-independent activity loss (Figure 5A,C).

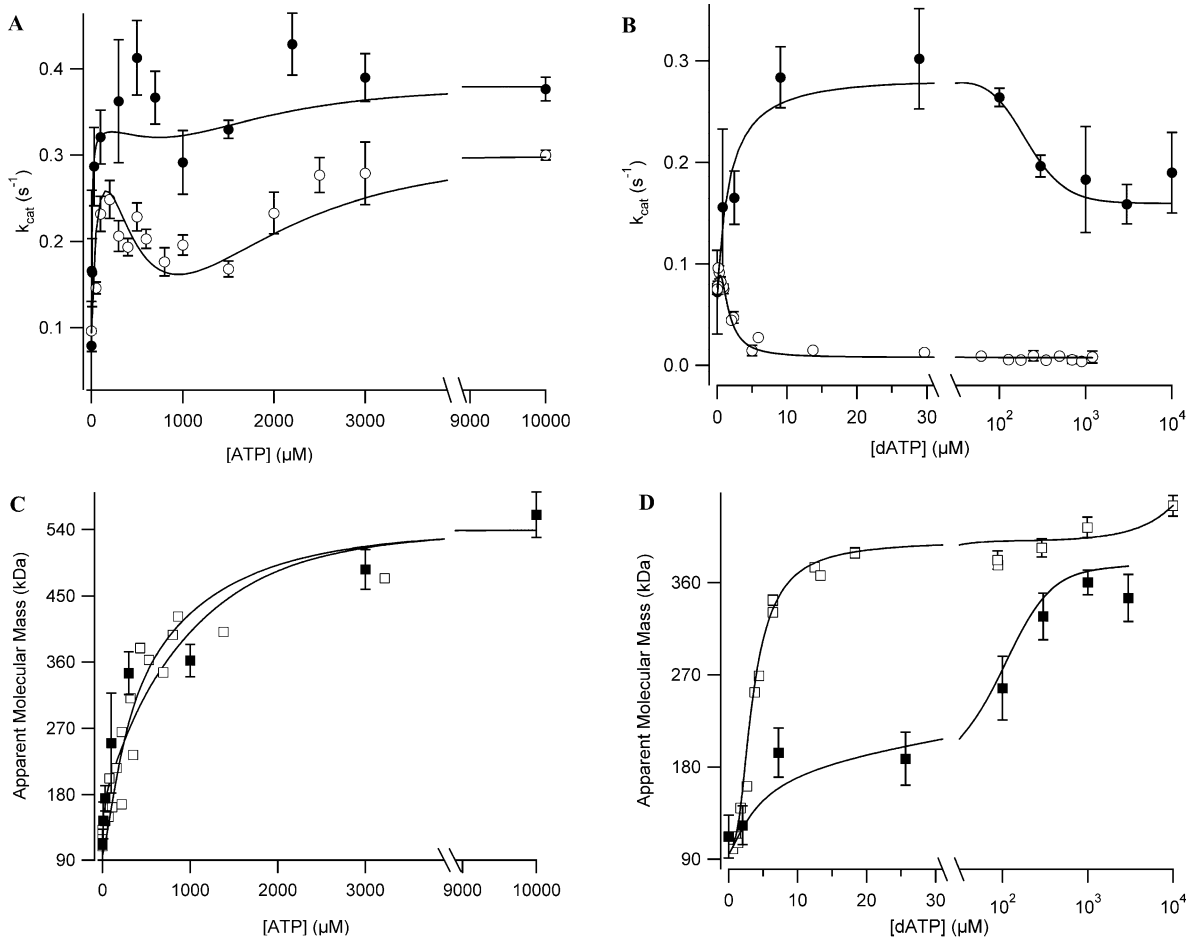

FIGURE 4: Dependence of CDP reductase and R1 molecular mass on ATP or dATP concentration. All solutions contained varying ATP or dATP concentrations as shown. The total Mg^{2+} concentration was 10 mM. Solutions for measuring CDP reductase activity also contained 1.2 μM D57N-mR1 or 1.2 μM wt-mR1 and 2.0 μM R2. (A) CDP reductase vs ATP [wt-mR1 and 1 mM CDP (○) and D57N-mR1 and 400 μM CDP (●)]. (B) CDP reductase vs dATP [wt-mR1 and 1.1 mM CDP (○) and D57N-mR1 and 400 μM CDP (●)]. (C) R1 molecular mass vs ATP [7.0 μM wt-mR1 and 1 mM CDP (□) and 5.0 μM D57N-mR1 and 400 μM CDP (■)]. (D) R1 molecular mass vs dATP [8.0 μM wt-mR1 (□) and 5.0 μM D57N-mR1 and 400 μM CDP (■)]. Each point is the average of two measurements ± the average deviation. D57N-mR1 data sets for panels A and C were fit simultaneously using Scheme 1, as were D57N-mR1 data sets for panels B and D. Data for wt-R1 at 10 mM Mg^{2+} and the corresponding solid line fits have been reprised from Kashlan et al. (*4*).

Effect of the D57N Mutation on Substrate K_m Values. Presented in Table 4 are K_m values determined from steady-state kinetic analysis of wt- and D57N-mR1. These results clearly show that the D57N mutation has a negligible effect on substrate affinity, as measured by K_m, whether measured by GDP reductase for the R1 dimer or by CDP reductase for the R1 hexamer.

dATP Effects on ATP-Saturated wt-mR1. The simplified model for allosteric regulation of mRR depicted in Scheme 1 does not directly address the question of whether the enzymatic activity and aggregation state of mR1 depend on ATP versus dATP occupation of the a-site. To investigate this question, we determined the effects on both CDP reductase activity and the apparent mR1 molecular mass of adding dATP to a solution containing 10 mM ATP (Figure 6A). In the presence of CDP, the ratios of dATP versus ATP affinities for the s-site (K_L), a-site ($K_{A'}$), and h-site ($K_{A''}$) have values of 40, 1000, and 0.03, respectively (Table 2), making it possible to displace ATP from the a-site while mostly retaining ATP in the s-site and not competing at all for ATP binding to the h-site. Addition of 0.1 mM dATP should result in ~90% occupancy by dATP of the a-site and 25% occupancy of the s-site. As seen in Figure 6A, addition of this amount of dATP leads to the striking result of a major loss (80%) in CDP reductase activity accompanied by only a minor loss in the apparent mR1 molecular mass (543 ± 40 to 514 ± 13 kDa). Since hexamer formation is totally dependent on ATP occupancy of the h-site, and all current evidence suggests no major differences arising from dATP versus ATP occupancy of the s-site (*4*), we interpret the loss of activity as arising principally from dATP substitution for ATP at the a-site within the mR1 hexamer, with a minor contribution arising from a small amount of tetramer formation as a result of ATP dissociation from the h-site. Thus, dATP displacement of ATP at the a-site both decreases the observed activity of the R1 hexamer and weakens ATP binding to the h-site, with $K_{A''}$ increasing from 2 to ~30 mM. As the dATP concentration is further increased, the activity falls further, and the apparent molecular mass decreases to a level intermediate between those of the hexamer and tetramer, similar to that which is seen in the presence of high concentrations of dATP (10 mM) in the absence of ATP (Figure 6A). Such high concentrations may afford partial h-site occupancy by dATP.

The activity experiments were generally carried out at subunit concentrations of 1.2 μM mR1 and 2.0 μM mR2. In

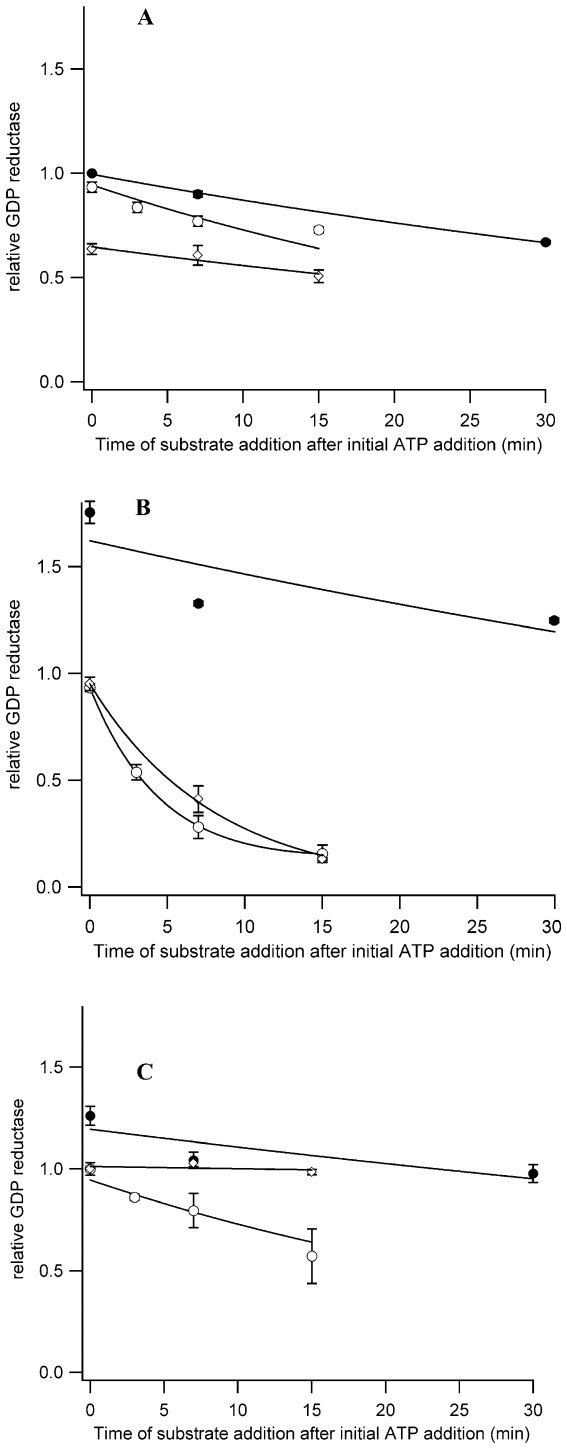

FIGURE 5: Effect of the D57N mutation on the preincubation effects of dTTP-dependent GDP reductase. Reaction mixtures containing 300 μM dTTP, 1.2 μM D57N-mR1 or 1.2 μM wt-mR1, 2.0 μM R2, and 10 mM Mg^{2+}, except as otherwise indicated, were preincubated for the times shown prior to the addition of 600 μM GDP. (A) In the absence of added ATP. Lines are drawn for first-order rate constants of 0.026 [wt-mR1 (○)], 0.014 [wt-mR1 and 3 mM Mg^{2+} (◇)], and 0.013 min^{-1} [D57N-mR1 (●)]}. (B) In the presence of 0.5 mM ATP. Lines are drawn for two parallel first-order rate constants of 0.24 and 0.026 min^{-1} [wt-mR1 (○)] and of 0.11 and 0.014 min^{-1} [wt-mR1 and 3 mM Mg^{2+} (◇)] and for a first-order rate constant of 0.010 min^{-1} [D57N-mR1 (●)]. (C) In the presence of 10 mM ATP. Lines are drawn for first-order rate constants of 0.026 [wt-mR1 (○)], 0.001 [wt-mR1 and 3 mM Mg^{2+} (◇)], and 0.008 min^{-1} [D57N-mR1 (●)]. Data for wt-mR1 at 10 mM Mg^{2+} and the corresponding solid line fits are reprised from Kashlan et al. (*4*).

Table 3: Reductase Rate Constants

rate constant	wild-type GDP	D57N GDP	wild-type CDP	D57N CDP
k_d (s^{-1})	0.28	0.27	0.29 (ATP)	0.33 ± 0.03 (ATP)
			0.25 (dATP)	0.29 ± 0.03 (dATP)
k_{4a} (s^{-1})	nd[a]	0.41 ± 0.01 (ATP)	nd[a]	0.34 ± 0.01 (ATP)
		0.48 ± 0.01 (dATP)		0.16 ± 0.01 (dATP)
k_h (s^{-1})	0.25	0.31	0.30	0.38

[a] Not determined.

Table 4: K_m Values

mR1	reductase activity	[ATP] (mM)	R1 aggregation state	K_m (μM)
wild-type	GDP[a]	0	dimer	4.9 ± 0.6[b]
D57N	GDP[a]	0	dimer	5.8 ± 0.6[c]
wild-type	CDP	3	hexamer	2.0 ± 0.3[d]
D57N	CDP	10	hexamer	1.6 ± 0.3[c]

[a] In the presence of saturating dTTP. [b] From Scott et al. (*3*). [c] From this work. [d] From Kashlan et al. (*4*).

the presence of 10 mM ATP, this concentration of mR2 is saturating (*4*). However, in the presence of 10 mM ATP and 0.1 mM dATP, the measured enzymatic activity is seen to rise 2-fold as the mR2 concentration is increased from 2 to 6 μM (Figure 6B). These latter data may be fit to a model identical to that introduced previously (eq 18 of ref *4*), in which three R2 dimers bind with a single intrinsic dissociation constant (K_d) to the R1 hexamer. The parameters derived using this model indicate that replacing ATP with dATP in the a-site of the R1 hexamer has little effect on RR specific activity (ATP, 0.30 s^{-1}, Table 3; dATP, 0.32 ± 0.06 s^{-1}) but increases K_d 50-fold [ATP, 0.066 ± 0.036 μM (*4*); dATP, 3.2 ± 1.1 μM]. Thus, most of the observed inhibition of RR enzymatic activity by 0.1 mM dATP in Figure 6A is due to a weakening of the binding of $mR2_2$ to $mR1_6$, rather than to a decrease in the specific activity of the holoenzyme.

Simulations of the Distribution of R1. To assess the relative importance of $mR1_2$ versus $mR1_6$ for activity in vivo, simulations of the distribution of R1 among the dimer, tetramer, and hexamer forms were performed using Scheme 1 and equilibrium constants determined previously (*3*, *4*), as well as the value of $K_{A''}$ for ATP of ~30 mM when the a-site is occupied with dATP. These simulations are presented in Figure 7 as a function of ATP concentration at a variety of R1 concentrations and a fixed dATP concentration of 10 μM, within the range of 1−60 μM reported for mammalian cells (*17*). They demonstrate that, within the cytosol, in which mR1 and ATP concentrations fall in the ranges of 1−5 μM (*18*, *19*) and 1−5 mM (*17*, *20*), respectively, $mR1_6$ is the major active form of R1. However, for cellular compartments containing much lower mR1 concentrations, in particular the nucleus, or for cells having abnormally low ATP levels, $mR1_2$ could be an important active form (see the Discussion).

Effects of Mg^{2+} Concentration. Our earlier experiments measuring wt-RR activity and wt-mR1 aggregation state (*3*, *4*) were carried out at 10 mM Mg^{2+} (total concentration), which ensured that virtually all added nucleoside di- and

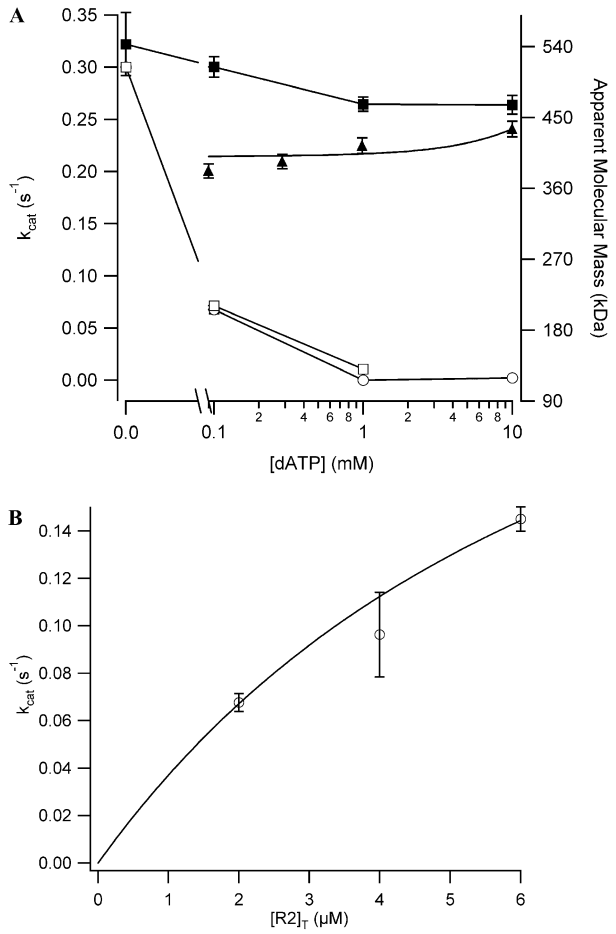

FIGURE 6: (A) Dependence of CDP reductase activity and mR1 molecular mass on added dATP in the presence of 10 mM ATP. Solutions for measuring CDP reductase activity contained 1.2 μM wt-R1, 2.0 μM D57N-mR1, and varying dATP concentrations as shown. dATP was added to the solutions either simultaneously with ATP addition (□) or 2 min after ATP addition (○). Following a 7 min preincubation with dATP, reactions were initiated by addition of 400 μM CDP. Each point is the average of two measurements ± the average deviation. Solutions for measuring the molecular mass of R1 by DLS contained 8.3 μM R1, 10 mM ATP, and varying dATP concentrations as shown (■). Data showing the molecular mass of mR1 as a function of dATP concentration in the absence of ATP (▲) are reprised from Kashlan et al. (*4*). (B) Dependence of CDP reductase activity on added mR2 at 10 mM ATP, 0.1 mM dATP, and 1.2 μM wt-R1. Reactions were carried out as described for panel A, with simultaneous addition of ATP and dATP.

triphosphates were present as the 1/1 Mg^{2+} complexes. In vivo Mg^{2+} concentrations have been reported to be 0.3−0.7 mM for free Mg^{2+} and 7 mM for total Mg^{2+} (*21*, *22*). Accordingly, we have repeated some of the key earlier experiments at lower Mg^{2+} concentrations, to assess the effects of such a change.

From Figure 3A, it is clear that dTTP-dependent GDP reductase activity in the absence of ATP is modulated by Mg^{2+} concentration. The results displayed in Figure 8A show that although such activity is not absolutely dependent on added Mg^{2+}, it does increase 2-fold as the Mg^{2+} concentration is increased, with an apparent dissociation constant for Mg^{2+} of 2.9 ± 1.2 mM. Comparable results have been reported earlier by others (*23*, *24*). Reducing $[Mg^{2+}]_T$ from 10 to 3 mM causes little qualitative change in the response of GDP reductase to added ATP (Figure 3A), although it is noteworthy that the minimum GDP reductase activity is reached at lower ATP concentrations. Like the results with GDP reductase, reducing $[Mg^{2+}]_T$ from 10 to 3 mM causes little qualitative change in ATP-induced aggregation when $[ATP]_T < [Mg^{2+}]_T$, except that aggregation occurs at lower ATP concentrations (Figure 8B). However, when $[ATP]_T$ is equal to $[Mg^{2+}]_T$ such that $[Mg^{2+}]_f$ is very low, R1 forms aggregates larger than the hexamer. It is also noteworthy that a low $[Mg^{2+}]_T$ (0.5 mM) favors R1 aggregation, even at a relatively low (100 μM) ATP concentration. Finally, as mentioned above, reducing $[Mg^{2+}]_T$ from 10 to 3 mM results in a 2-fold decrease in the rate of formation of $R1_{4b}$ from $R1_{4a}$ (Figure 5B). These results indicate that Scheme 1 is valid over a range of $[Mg^{2+}]_T$ values that include in vivo concentrations, although the values of some of the equilibrium constants characterizing Scheme 1 are clearly affected by the Mg^{2+} concentration.

DISCUSSION

Effects of the D57N Mutation. The comprehensive model suggests a straightforward rationale for the dramatic qualitative activity differences observed between mR1 and the D57N-mR1 variant. According to this rationale, D57N-mR1 does not isomerize from $R1_{4a}$ to $R1_{4b}$ (Scheme 1), with, as a corollary, that $R1_{4a}$ forms an enzymatically active complex with $R2_2$, a point that was not clear from our earlier studies (*4*). The activity results in Figures 3−5 can then be explained on the basis that binding of either ATP or dATP to the a-site of D57N-mR1 induces formation of $R1_{4a}$ but not of $R1_{4b}$, although it is unclear whether the failure to form $R1_{4b}$ is due more to an increased kinetic barrier for $R1_{4b}$ formation or to a shift in equilibrium between $R1_{4b}$ and $R1_{4a}$. This dramatic effect of D57N mutation, along with two earlier observations with wt-R1, leads us to conclude that $R1_{4b}$ formation from $R1_{4a}$ is exquisitely sensitive to the details of dATP interaction with the a-site. Thus, $R1_{4b}$ formation occurs much more rapidly with dATP versus ATP bound to the a-site (*4*). Moreover, although both dTTP and dGTP can induce R1 tetramer formation, albeit at very high, nonphysiological, concentrations, such R1 tetramer formation is not accompanied by a loss of RR activity (*4*), presumably reflecting an inability of $R1_{4a}$ formed on a-site binding to convert to $R1_{4b}$.

The D57N mutation stabilizes $R1_{4a}$ relative to $R1_2$ and $R1_6$, as shown by its effects on K_t (130-fold decrease) and K_h (70-fold increase) (Table 2). These effects are not unexpected, given the presence of residue 57 within the a-site at the dimer−dimer interface which is integral to both mR1 tetramerization and hexamerization (*4*, *11*). On the other hand, the D57N mutation hardly affects (~2-fold) the overall dissociation constant for formation of R1 dimers from the R1 hexamer, which is given by K_tK_h.

The D57N mutation also has only minor effects on the specific activities of the $mR2_2$ complexes of both the mR1 dimer and mR1 hexamer (Table 3). However, for the D57N variant, it is worth noting the apparent greater interplay with substrate when dATP versus ATP is bound to the a-site. Thus, the k_{4a}/k_d ratio changes from 1.8 to 0.6 for GDP reductase as compared with CDP reductase in the presence of dATP, whereas the corresponding numbers in the presence of ATP are 1.5 and 1.0, respectively.

While the D57N mutation has little effect on substrate affinity, as measured by K_m (Table 4), it strongly affects

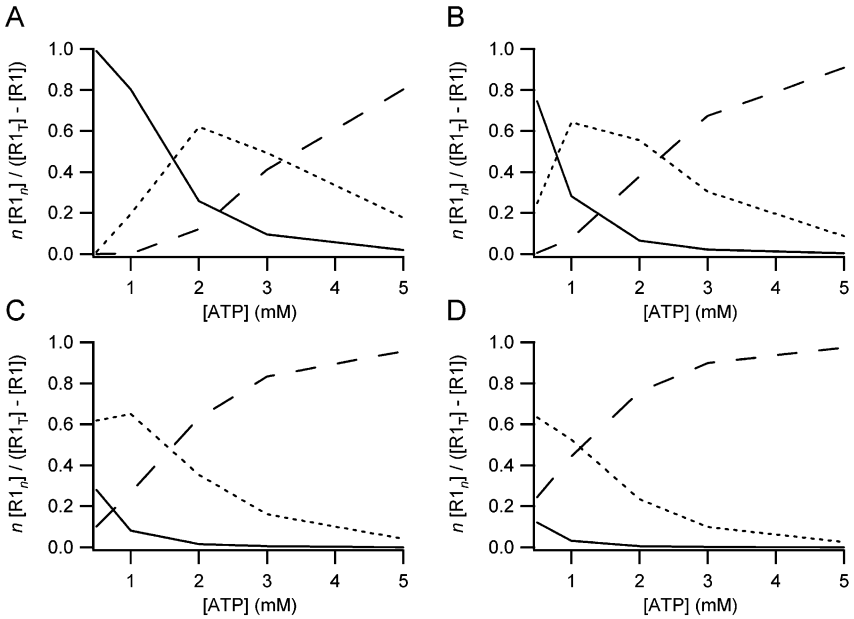

FIGURE 7: Distribution of R1 as $R1_2$ (—), $R1_4$ (•••), or $R1_6$ (– – –) simulated as described in Experimental Procedures. Simulations were performed at 10 μM dATP, varying ATP concentrations as shown, and (A) 0.01, (B) 0.1, (C) 1, or (D) 5 μM $[R1]_T$.

allosteric ligand binding, providing evidence not only for the direct and expected involvement of this residue at the a-site but also for interaction between the a- and s-sites. Some of these effects depend on whether binding is measured in the presence of dTTP/GDP or CDP, which, given the apparent lack of effect on substrate binding, we interpret as being due to the presence of dTTP at the s-site. The most marked differences are at the a-site ($K_{A'}$), where the effect of the mutation is to decrease dATP affinity by 8-fold in the presence of dTTP/GDP and 300-fold in the presence of CDP while increasing ATP affinity by 7- and 3-fold, respectively. As a result of these changes, in D57N-mR1 the a-site binds ATP and dATP with similar affinities, a dramatic change from the strong preference for dATP in wt-mR1. ATP and dTTP affinity for the s-site (K_L) is also increased by the D57N mutation (from 5- to 10-fold), while dATP affinity is little affected. Finally, the D57N mutation has modest and variable effects on ATP binding to the h-site ($K_{A''}$), increasing the affinity 3-fold in the presence of dTTP/GDP, while decreasing the affinity 2-fold in the presence of CDP.

dATP versus ATP at the a-Site. Although either dATP or ATP binding to the a-site of wt-mR1 induces inactive $R1_{4b}$ formation (Scheme 1), our results show important differences in R1 properties when the a-site is occupied by dATP rather than ATP. These include more rapid $R1_{4b}$ formation from $R1_{4a}$, weaker binding of $mR2_2$ to the mR1 hexamer, and weaker ATP binding to the h-site. These differences provide specific mechanisms by which the dATP/ATP ratio in mammalian cells (*17*) can modulate in vivo RR enzymatic activity (*4*).

Comprehensive Model and RR Activity in Vivo. There are two important active forms of the wt-RR holoenzyme, $mR1_2$-$mR2_2$ and $mR1_6mR2_j$ (*4*). The stoichiometry of mR2 bound to the mR1 hexamer, *j*, is not specified because RR activity in the cell is typically limited by the level of R2 (*19*), which, even at its maximum in the S phase, does not exceed 0.5−0.8 μM (*25*, *26*). As a result, $mR1_6$ is unlikely to be saturated ($j = 6$) with $mR2_2$ in vivo, and *j* will vary with cell cycle. The comprehensive model permits quantitative estimates to be made of the distribution of R1 between $mR1_2mR2_2$ and $mR1_6mR2_j$ as a function of allosteric ligand and R1 concentrations (Figure 7). This capability allows us to address the question of which is likely to be dominant in vivo. Because RR is a target for chemical chemotherapy (*27*, *28*), resolution of this question has potential significance for the design and testing of RR inhibitors, which may show differential activity toward $mR1_2mR2_2$ and $mR1_6mR2_j$.

As indicated above, our simulations clearly suggest that $mR1_6mR2_j$ is the dominant active form of RR in the cytosol of normal cells, where the large majority of RR activity in mammals is found (*29*−*32*). However, it is quite possible that $mR1_2$ is present in amounts equal to or larger than the amount of $mR1_6$ in the nucleus, where there has long been evidence for the presence of at least small amounts of RR activity (*29*, *33*, *34*). Moreover, the case for nuclear RR activity has been strengthened by the recent characterization of a p53-dependent R2 gene, p53R2, the product of which (a) is localized in the nucleus, (b) is 80% identical with cytoplasmic mR2, (c) is believed to be important for the urgent supply of dNTPs for DNA repair at arrested G1 and G2 phases, in contrast to cytoplasmic mR2 which is involved in normal DNA replication during S phase, and (d) forms active RR in vitro on complexation with mR1 (*35*−*38*). If nuclear R1 concentrations fell in the range of 0.01−0.1 μM or below, the simulations indicate that $mR1_2mR2_2$ would be the major active form of RR in the nucleus.

$mR1_2$ could also make a major contribution to total active RR in cells having abnormally low ATP levels. In this connection, the approach to cancer therapy that relies on ATP depletion in tumor cells (*39*, *40*) is of particular interest, it having been demonstrated that 6-aminonicotinamide and 6-methylmercaptopurine riboside, added in combination, lower ATP levels in tumor cells to ≤15% (∼0.3 mM) of that found in normal cells (*17*, *20*). Thus, an RR inhibitor that specifically targets $mR1_2mR2_2$ might be highly selective for inhibiting the proliferation of ATP-depleted tumor cells.

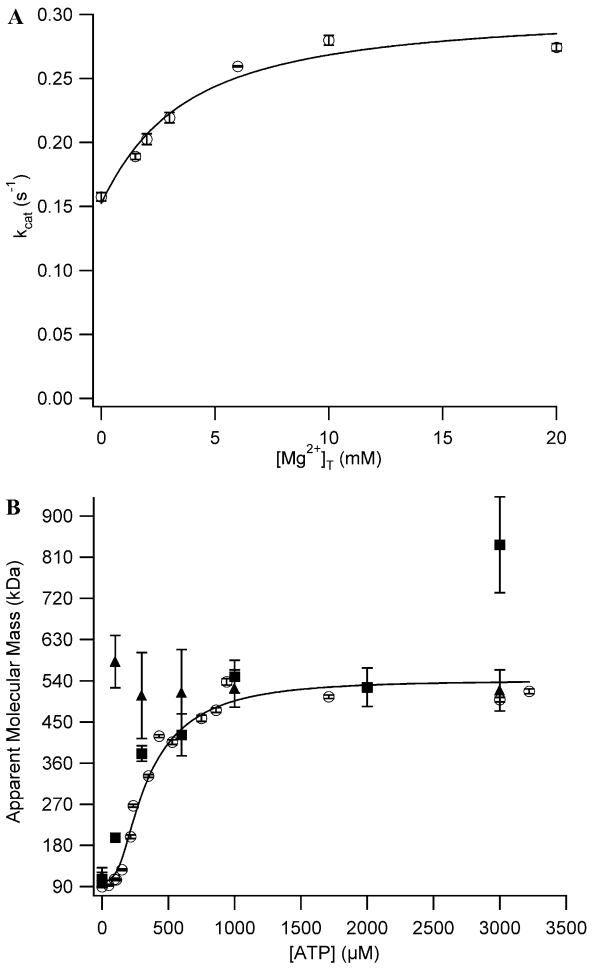

FIGURE 8: Mg^{2+} dependence. (A) Dependence of wt-GDP reductase on $[Mg^{2+}]_T$. Solutions for measuring GDP reductase activity contained 1.2 μM wt-mR1, 2.0 μM R2, 0.3 mM dTTP, and varying Mg^{2+} concentrations as shown. (B) Dependence of R1 molecular mass on ATP at various $[Mg^{2+}]_T$ values: 0.5 (▲), 3.0 (■), and 10 mM (○). Data for wt-mR1 at 10 mM Mg^{2+} and the corresponding solid line fit are reprised from Kashlan et al. (*4*).

Comparison with Other Work. A comparison of the catalytic and ligand binding activities of D57N-mR1 and wt-mR1, partially overlapping some of the experiments reported in this work, has been published by Reichard et al. (*7*). Although the significance of this earlier work is diminished somewhat by its use of incompletely purified and somewhat unstable preparations of D57N-mR1, and limited by a failure to explicitly consider the effects of nucleotide-dependent oligomeric-state changes, some important consistencies between the two studies are apparent. These include the findings that (a) for both wt-mR1 and D57N-mR1, low concentrations of ATP and dATP stimulate the reduction of CDP while dTTP stimulates the reduction of GDP; (b) dATP binds a second allosteric site which inhibits wt-mR1 enzymatic activity and stimulates D57N-mR1 enzymatic activity; (c) the D57N mutation decreases the affinity of dATP for at least one of these sites; and (d) the enzymatic activities of both wt-mR1 and D57N-mR1 have biphasic responses to increasing ATP concentrations when the s-site is occupied with dTTP. This latter result provides strong evidence for two allosteric sites (i.e., the a- and h-sites) in addition to the s-site, in accord with the comprehensive model.

There are, however, two important disagreements, with respect to both the results themselves and their interpretation, which we would like to highlight. The first concerns the effect of ATP on the dTTP-dependent GDP reductase activity of $R2_2$ complexes of wt- and D57N-mR1. Reichard et al. (*7*) report very similar results for both wt- and D57N-mR1: little change in enzymatic activity as the concentration of ATP is increased from 0 to 0.4 mM, followed by a large (4−5-fold) and very sharp increase in enzymatic activity when the ATP concentration is increased from 0.4 to 1 mM, with little or no further increase as the ATP concentration is increased to 2 mM. This dependence is quite different from what we report in Figure 3A. However, it is important to recognize that, qualitatively at least, these observed differences derive principally from a single source, i.e., the activity measured in the absence of added ATP. For both wt- and D57N-mR1, we find this activity to be similar to that measured at saturating ATP concentrations (at 10 mM Mg^{2+}), whereas Reichard et al. (*7*) report much lower values. Although the source of this discrepancy is unclear, three potential factors are worth mentioning. One is Mg^{2+} concentration. Results presented in Figure 3 show that the activity of the R1 dimer present in the absence of ATP is much more sensitive to the Mg^{2+} concentration than that of the R1 hexamer present formed in the presence of added ATP. While this sensitivity is insufficient (Figure 8A) to account for all of the discrepancy, it may be a contributing factor. The other two potential factors are the time of preincubation prior to initiation of the reaction with substrate (Figure 5) [neither Mg^{2+} concentration nor preincubation time is clearly specified by Reichard et al. (*7*)] and the differences in mR1 purification, with Reichard et al. employing a dATP−Sepharose column, with an attendant risk that the ATP used to elute mR1 is incompletely removed, while we use a peptide affinity column.

The second major disagreement concerns the effect of the D57N mutation on decreasing the extent of dATP binding to one of the allosteric sites. As noted above (see Table 2), our results clearly implicate the a-site as being the principal one affected, with s-site binding remaining relatively unchanged. In contrast, Reichard et al., in reporting results of direct binding studies that are ambiguous due to uncertainties in the values of active R1 concentrations, reach the conclusion that the D57N mutation affects dATP binding to the s-site rather than the a-site, which necessitates dissociation constants to each site of <1 μM. However, this conclusion appears to be inconsistent with their own results showing GDP and CDP reductase to be strongly modulated by dATP concentrations in the range of 100−500 μM. Here it should be noted that Reichard et al. (*7*) could also explain their dATP binding data assuming a moderate weakening of s-site binding and a major weakening of a-site binding, an interpretation much more in agreement with our own.

ACKNOWLEDGMENT

We gratefully acknowledge Lars Thelander for providing the pETD57NR1 vector, Dr. Paul Janmey for help with DLS measurements, and Nora Zuño for performing bacterial growth.

REFERENCES

1. Jordan, A., and Reichard, P. (1998) *Annu. Rev. Biochem. 67*, 71−98.

2. Stubbe, J., and van der Donk, W. A. (1995) *Chem. Biol. 2*, 793−801.
3. Scott, C. P., Kashlan, O. B., Lear, J. D., and Cooperman, B. S. (2001) *Biochemistry 40*, 1651−1661.
4. Kashlan, O. B., Scott, C. P., Lear, J. D., and Cooperman, B. S. (2002) *Biochemistry 41*, 462−474.
5. Larsson, K. M., Andersson, J., Sjoberg, B. M., Nordlund, P., and Logan, D. T. (2001) *Structure 9*, 739−750.
6. Thelander, L., and Reichard, P. (1979) *Annu. Rev. Biochem. 48*, 133−158.
7. Reichard, P., Eliasson, R., Ingemarson, R., and Thelander, L. (2000) *J. Biol. Chem. 275*, 33021−33026.
8. Ullman, B., Gudas, L. J., Caras, I. W., Eriksson, S., Weinberg, G. L., Wormsted, M. A., and Martin, D. W., Jr. (1981) *J. Biol. Chem. 256*, 10189−10192.
9. Eriksson, S., Gudas, L. J., Ullman, B., Clift, S. M., and Martin, D. W., Jr. (1981) *J. Biol. Chem. 256*, 10184−10188.
10. Uhlin, U., Uhlin, T., and Eklund, H. (1993) *FEBS Lett. 336*, 148−152.
11. Eriksson, M., Uhlin, U., Ramaswamy, S., Ekberg, M., Regnstrom, K., Sjoberg, B. M., and Eklund, H. (1997) *Structure 5*, 1077−1092.
12. Davis, R., Thelander, M., Mann, G. J., Behravan, G., Soucy, F., Beaulieu, P., Lavallee, P., Graslund, A., and Thelander, L. (1994) *J. Biol. Chem. 269*, 23171−23176.
13. Mann, G. J., Graslund, A., Ochiai, E., Ingemarson, R., and Thelander, L. (1991) *Biochemistry 30*, 1939−1947.
14. Yang, F. D., Spanevello, R. A., Celiker, I., Hirschmann, R., Rubin, H., and Cooperman, B. S. (1990) *FEBS Lett. 272*, 61−64.
15. Eriksson, S. (1983) *J. Biol. Chem. 258*, 5674−5678.
16. Chimploy, K., and Mathews, C. K. (2001) *J. Biol. Chem. 276*, 7093−7100.
17. Traut, T. W. (1994) *Mol. Cell. Biochem. 140*, 1−22.
18. Chang, C. H., and Cheng, Y. C. (1979) *Cancer Res. 39*, 436−442.
19. Engstrom, Y., Eriksson, S., Jildevik, I., Skog, S., Thelander, L., and Tribukait, B. (1985) *J. Biol. Chem. 260*, 9114−9116.
20. Kennedy, H. J., Pouli, A. E., Ainscow, E. K., Jouaville, L. S., Rizzuto, R., and Rutter, G. A. (1999) *J. Biol. Chem. 274*, 13281−13291.
21. Iotti, S., Frassineti, C., Alderighi, L., Sabatini, A., Vacca, A., and Barbiroli, B. (2000) *Magn. Reson. Imaging 18*, 607−614.
22. Li, W., Zheng, T., Babu, A. N., Altura, B. T., Gupta, R. K., and Altura, B. M. (2001) *Brain Res. Bull. 56*, 153−158.
23. Engstrom, Y., Eriksson, S., Thelander, L., and Akerman, M. (1979) *Biochemistry 18*, 2941−2948.
24. Kuzik, B. A., and Wright, J. A. (1979) *Enzyme 24*, 285−293.
25. McClarty, G. A., Chan, A. K., Engstrom, Y., Wright, J. A., and Thelander, L. (1987) *Biochemistry 26*, 8004−8011.
26. Wright, J. A., Alam, T. G., McClarty, G. A., Tagger, A. Y., and Thelander, L. (1987) *Somatic Cell Mol. Genet. 13*, 155−165.
27. Szekeres, T., Fritzer-Szekeres, M., and Elford, H. L. (1997) *Crit. Rev. Clin. Lab. Sci. 34*, 503−528.
28. Robins, M. J. (1999) *Nucleosides Nucleotides 18*, 779−793.
29. Chang, C. H., and Cheng, Y. C. (1979) *Cancer Res. 39*, 5087−5092.
30. Engstrom, Y., Rozell, B., Hansson, H. A., Stemme, S., and Thelander, L. (1984) *EMBO J. 3*, 863−867.
31. Leeds, J. M., Slabaugh, M. B., and Mathews, C. K. (1985) *Mol. Cell Biol. 5*, 3443−3450.
32. Engstrom, Y., and Rozell, B. (1988) *EMBO J. 7*, 1615−1620.
33. Larsson, A. (1969) *Eur. J. Biochem. 11*, 113−121.
34. Reddy, C. C., Thomas, C. E., Scholz, R. W., and Massaro, E. J. (1982) *Biochem. Biophys. Res. Commun. 107*, 75−81.
35. Nakano, K., Balint, E., Ashcroft, M., and Vousden, K. H. (2000) *Oncogene 19*, 4283−4289.
36. Tanaka, H., Arakawa, H., Yamaguchi, T., Shiraishi, K., Fukuda, S., Matsui, K., Takei, Y., and Nakamura, Y. (2000) *Nature 404*, 42−49.
37. Guittet, O., Hakansson, P., Voevodskaya, N., Fridd, S., Graslund, A., Arakawa, H., Nakamura, Y., and Thelander, L. (2001) *J. Biol. Chem. 276*, 40647−40651.
38. Yamaguchi, T., Matsuda, K., Sagiya, Y., Iwadate, M., Fujino, M. A., Nakamura, Y., and Arakawa, H. (2001) *Cancer Res. 61*, 8256−8262.
39. Martin, D. S., Bertino, J. R., and Koutcher, J. A. (2000) *Cancer Res. 60*, 6776−6783.
40. Martin, D. S., Spriggs, D., and Koutcher, J. A. (2001) *Apoptosis 6*, 125−131.

BI020634D